Spatial variability of marine heatwaves in the Chesapeake Bay

Authors:

Rachel Wegener	University of Maryland, College Park	rwegener@umd.edu
Jacob Wenegrat	University of Maryland, College Park	wenegrat@umd.edu
Veronica Lance	National Oceanic and Atmospheric Administration (NOAA) National Office of Satellite Data and Information Service,Center for Satellite Applications and Research, and NOAA Coastwatch	veronica.lance@noaa.gov
Skylar Lama	School of Earth and Atmospheric Science and the Program of Ocean Science and Engineering, Georgia Institute of Technology	slama8@gatech.edu

Version: 2

Peer review status: This is a non-peer-reviewed preprint submitted to EarthArXiv.

Spatial variability of marine heatwaves in the Chesapeake Bay

Rachel Wegener[1*], Jacob Wenegrat[1], Veronica P. Lance[2], Skylar Lama[3, 4]

[1*]Department of Atmospheric and Oceanic Science, University of Maryland, College Park, 4254 Stadium Drive, College Park, 20742, MD, USA.

[2]National Oceanic and Atmospheric Administration (NOAA) National Office of Satellite Data and Information Service,Center for Satellite Applications and Research, and NOAA Coastwatch,, 5830 University Research Court, College Park, 20740, MD, USA.

[3]School of Earth and Atmospheric Science, Georgia Institute of Technology, 311 Ferst Dr, Atlanta, 30332, GA, USA.

[4]Ocean Science and Engineering, Georgia Institute of Technology, 311 Ferst Dr, City, 30332, Atlanta, GA.

*Corresponding author(s). E-mail(s): rwegener@umd.edu; Contributing authors: wenegrat@umd.edu; veronica.lance@noaa.gov; slama8@gatech.edu ;

Abstract

The Chesapeake Bay is the largest estuary in the continental United States. Extreme temperature events, termed marine heatwaves, are impacting this ecologically important zone with increasing frequency. Although marine heatwaves evolve across space and time, a complete spatial picture of marine heatwaves in the Bay is missing. Here we use satellite sea surface temperature to characterize marine heatwaves in the Chesapeake Bay. We consider three products: NASA MUR, NOAA Geo-Polar, and Copernicus Marine OSTIA, and validate their effectiveness using in situ data from the Chesapeake Bay Program. We find that Geo-Polar SST is the most suitable dataset for marine heatwave analysis in this location, with an root mean squared error of 1.6°C. Marine heatwaves occur on average of 2.3 times per year and last 10.8 days per event. A north-south (along estuary) gradient is identified as a common pattern of spatial variability. Seasonally, summer marine heatwaves are shorter, more frequent, and have a more consistent duration, with an inter-quartile range of 6-11 days (median=8 days). December marine heatwaves have a much larger inter-quartile range of 6-28 days (median=13 days). Marine heatwaves are increasing at a rate of 4 events/year in the upper Bay and 2 events/year in the main stem of the lower Bay. Our analysis suggests that the major observed spatial patterns are a result of long term warming, not shifts in the spread of the temperature distribution. Overall, the qualitative character of marine heatwaves in the Chesapeake Bay is not changing but they are becoming more frequent.

Keywords: marine heatwaves, sea surface temperature, estuary, Chesapeake Bay, satellite remote sensing

1 Introduction

Anthropogenic activities have warmed the surface ocean, with signs of surface warming going back to at least the mid-1950s (Tyrell, 2011). In addition to increasing average temperatures, prolonged periods of anomalously hot water, termed marine heatwaves (MHW), have been on the rise (Oliver et al, 2019). Extreme temperature events such as MHWs affect marine ecosystems on the individual, population, and community levels (Smith et al, 2023), but ecosystem response can differ based on the characteristics of the MHW such as duration and rate of onset (Smith et al, 2023). These ecosystem impacts translate into socioeconomic impacts. In the US alone, economic losses "...exceed US$800 million in direct losses and in excess of US$3.1 billion per annum in indirect losses for multiple consecutive years" from MHW events (through October 2022)(Smith et al, 2021). MHWs and their ecological and economic impact are unfortunately part of our warming world.

Efforts to study MHW with satellite imagery have been undertaken for study areas around the world (see: Mohamed et al, 2022; Chatterjee et al, 2022; Huang et al, 2021; Oliver et al, 2018). Satellite imagery provides a temporally consistent data source over a broad spatial scale, making it a strong data product for the analysis of MHW. While more difficult, past work has also investigated MHW in the coastal ocean. Marin et al (2021)'s global coastal MHW analysis showed increasing numbers of MHW events, with concentrated increased in hotspots. One of the identified hotspots is the northeastern US coast, home to the Chesapeake Bay.

The Chesapeake Bay is the largest and one of the most productive estuaries in the continental United States (Bilkovic et al, 2019) (Figure 1). The Chesapeake Bay has seen a trend of long term warming (Hinson et al, 2022; Ding and Elmore, 2015) and increasing temperatures have been linked to growing hypoxic conditions in the Bay (Du et al, 2018). In addition to long term warming, previous work has identified MHWs in the Chesapeake Bay using buoy data (Mazzini and Pianca, 2022; Shunk et al, 2024). Extreme temperatures in 2005 caused an over 50% loss in the seagrass species *Z. marina* in which fisheries species find nursery habitat (Lefcheck et al, 2017). As a result, the area saw declines in three commercially important fish species (Smith et al, 2023). A report by the Scientific and Technical Advisory Committee, an independent

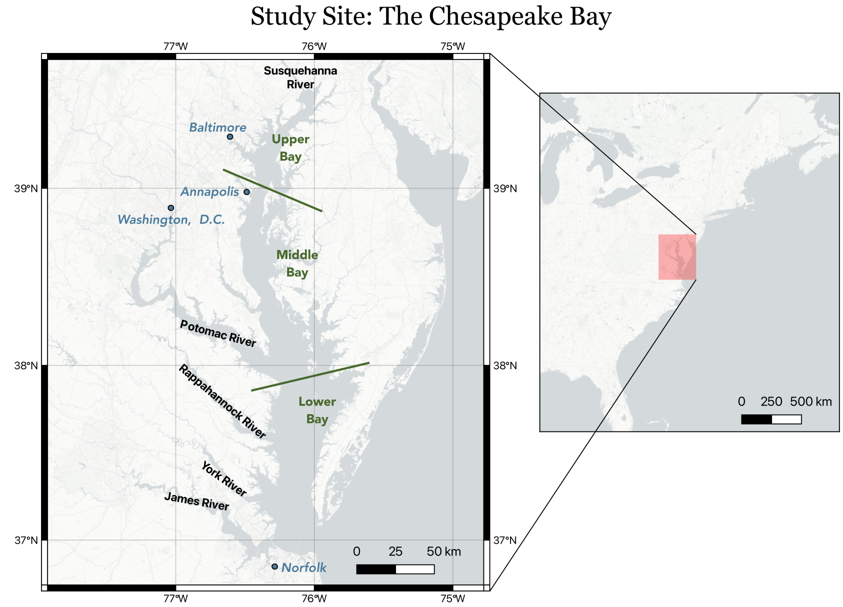

Fig. 1 A map of the Chesapeake Bay, including major rivers referenced throughout this study.

group which provides scientific and technical guidance on environmental issues in the Chesapeake Bay, specifically highlighted the need to develop a marine heatwave warning system due to the impact on living resources (Batiuk et al, 2023).

Here we use sea surface temperature (SST) satellite data to evaluate the occurrence and characteristics of MHWs in the Chesapeake Bay over a 21 year period, looking at average characteristics as well as long term trends. We specifically focus on patterns in the characteristics of MHWs including duration, maximum intensity, cumulative intensity, and rates of onset and decline. MHW characteristics are critical for assessing the potential ecological impact, and as potential guidance towards understanding the physical causes of MHW. Furthermore, we investigate Chesapeake Bay MHW using observations at a new level of geographic detail, as satellite data enables spatial coverage that is not possible with in situ data alone. Past work using buoys did not find significant differences between the surface expressions of MHW characteristics in the different regions of the Chesapeake Bay (Mazzini and Pianca, 2022), however we find that there is spatial variation in the surface expression of several defining characteristics of MHWs. Finally, the use of satellite data to investigate MHWs in an estuary setting is novel. Despite the relatively limited horizontal resolution of the observations relative to the size of the Bay, the results and validation presented here suggest this approach can be useful for understanding both temporal and spatial variability of MHWs in estuarine ecosystems such as the Chesapeake Bay.

In section 2 we introduce the chosen datasets and describe the definition of MHWs and MHW characteristics. In section 3 we discuss the validation of the satellite data. We also discuss the spatial and temporal patterns in MHWs characteristics. In section

4 we conclude by summarizing our major findings and propose routes for future analysis.

2 Methods

2.1 Satellite Data Sources

The satellite data products potentially suitable for this study are those with a fine spatial grid, a daily frequency, and a long operating period. The need for high spatial grid is driven by the size of the Chesapeake Bay. The need for a daily frequency is due to the 5 day length definition for a MHW. Finally, the need for a long operating period is driven by the baseline climatology required for MHW calculations. Hobday et al (2016) recommends a 30 year climatology. However, past work has shown no appreciable difference in MHW duration or intensity calculated from climatologies based on records as short as 10 years when compared with those calculated using the recommended 30 year time series (Schlegel et al, 2019).

Three satellite SST products fulfilling these criteria were evaluated as candidates for this study: NASA MUR v4.1, NOAA Geo-Polar Blended v2.0, and Copernicus Marine OSTIA v1.3.5. NASA MUR is a daily ∼1km level 4 product based on nighttime SST observations and provides an estimate of the foundation temperature (Chin et al, 2017). Foundation temperature, as defined by the Group for High Resolution Sea Surface Temperature (GHRSST), is the temperature at a depth free of diurnal variability (Donlon et al, 2007). NOAA Geo-Polar is also a daily level 4 product, and has ∼5km grid resolution (Maturi et al, 2017). Copernicus Marine OSTIA is a daily level 4 product which also has ∼5km grid resolution (E.U. Copernicus Marine Service Information (CMEMS), 2023; Donlon et al, 2012). These level 4 products provide variables derived from a combination of multiple other measurements (The Group for High Resolution Sea Surface Temperature Science Team et al, 2022). Geo-Polar provides estimates of both daytime and nighttime SST. In this study nighttime SST is used to more closely estimate the foundation temperature for comparison with NASA MUR and Copernicus Marine OSTIA. See Table 1 for a summary of the three datasets. All datasets are gap filled such that any no-data values (ex. data gaps caused by clouds) are filled in by spatial and temporal interpolation with estimated SST values. Seven days of data in the Geo-Polar dataset were removed by NOAA data processing due to quality control, as were 3 days of the MUR dataset. These missing days were linearly interpolated in time for each pixel when generating the climatology.

2.2 Marine Heatwave Calculation, Characteristics, and Long Term Trends

Hobday et al (2016) established the canonical definition of a MHW: a MHW occurs when the temperature rises above the 90th percentile temperature for that day and persists above the daily 90th percentile value for at least 5 days. This is illustrated in Figure 2 panel A. If an event exceeds the 90th percentile threshold but does not last 5 days it is called a heat spike. The time period for the climatology is the full dataset time period, Jan. 1, 2003 to Dec. 31, 2023 (21 years). Again following Hobday et al

Table 1 Satellite SST Data Sources

Product Name	Version	Organization	Spatial Grid	Temporal Resolution	Availability
MUR	4.1	NASA	$0.01°(\sim 1km)$	daily	May 31, 2002 - present
Geo-Polar Blended	2.0	NOAA	$0.05°(\sim 5km)$	daily	Sept. 1, 2002 - present
OSTIA	1.3.5	Copernicus Marine	$0.05°(\sim 5km)$	daily	Dec. 31, 2006 - present

(2016), the 90th percentile threshold for each day uses the days from a centered 11 day window. After the threshold is calculated, the values are smoothed using a 31 day moving average. If multiple MHW longer than 5 days occur within two days of each other they are considered to be a single MHW event. MHWs were calculated using the Python software package marineHeatWaves (Oliver, 2023). The procedures described above are the defaults of this package, and are consistent with the recommendations in Hobday et al (2016).

In addition to identifying MHW, the MHW processing computes a variety of MHW characteristics, which allow us to consider different types of MHW. Two extreme temperature events could both be MHW, but still have very different characteristics and thus correspond to different ecological impacts or physical processes of development. The 6 characteristics analyzed in this study are: 1) number of annual events, 2) duration, 3) maximum intensity, 4) cumulative intensity, 5) rate of onset, and 6) rate of decline. Figure 2 panel B shows a graphic representation of the MHW characteristics for an example heatwave in July 2020 (see also Hobday et al, 2016).

While most of the analysis presented here used the MHW definition from Hobday et al (2016), we also performed our analysis using a linearly detrended SST baseline to remove the long term warming signal. To do this we performed a linear fit on the raw satellite SST timeseries, then subtracted the linear trend from the SST. After removing the long term trend the remainder of the MHW calculation was calculated as described in the previous paragraph. These results are discussed in section 3.3 below.

To aid in understanding changes over time an analysis of long term trends in MHW characteristics is performed. Each pixel in this analysis is treated as an independent time series. Each time series is grouped into annual bins and average MHW characteristics are computed per year. These annual values were then fit to a linear trend and the slope and significance were calculated for the 21 year times series. Significance testing was performed using a one-sided student t-test on each pixel in the bay and spatial patterns were evaluated using multiple hypothesis testing (Wilks, 2016). Multiple hypothesis testing accounts for the number of false positive trends that would be expected in a sample of our size using a false discovery rate, in this study set to 10%.

2.3 Satellite Data Validation

In situ data compiled by the Chesapeake Bay Program (CBP) was used to validate satellite SST in the Chesapeake Bay (Chesapeake Bay Program, 2020). The database

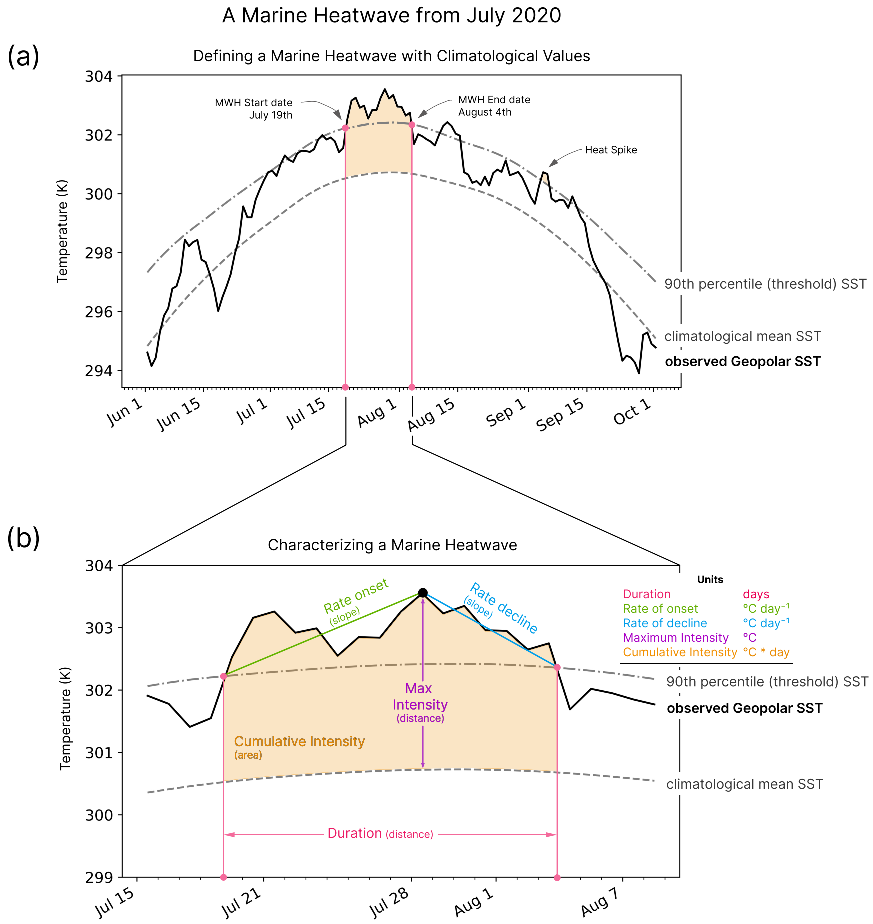

Fig. 2 The observed and climatological values of a MHW from July 2020 in the Tangier Sound in the Middle Chesapeake Bay (38.03°N, 75.97°W), illustrating the definitions of a MHW and MHW characteristics defined in Hobday et al (2016). Panel (a) visualizes a sustained temperature anomaly exceeding the 90th percentile threshold value defining a MHW. Panel (b) shows SST focused on the heatwave period, labeling the 5 MHW statistics used in this study to characterize MHWs.

contains measurements from the CBP partner organizations at long-term, fixed monitoring stations, including ship-based observations. *Traditional Partner Data* from all the programs was used.

The satellite datasets all estimate foundation SST. The in situ data, on the other hand, provide measurements of SST at multiple times of day and depths. To approximate the foundation temperature values from the in situ dataset, only temperature values between 1 and 3 meters depth were used. This was done to avoid very

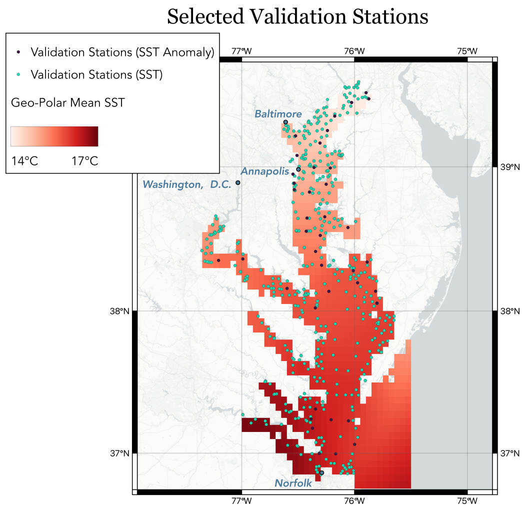

Fig. 3 Locations of CBP validation stations for evaluating the SST (green points) and the SST anomaly (purple points). Underlying imagery is the mean Geo-Polar SST from the study time period of Jan. 1, 2003 to Dec. 31, 2022.

near-surface measurements, which are likely subject to stronger diurnal temperature fluctuations. The sensitivity of this depth choice was tested by computing the RMSE between in situ and satellite SST values with several depth choices ranging from 0.5-7m. The RMSE changed by 0.1°C or less in all depth choices. The validation period was a 21 year period from Jan. 1, 2003 to Dec. 31, 2023.

Two subsets of the CBP data were used for validation. The first subset is comprised of 483 stations used to validate the SST observations from the satellites. This was done to get an understanding of raw dataset error and may additionally provide insight for other potential uses of satellite SST in the Chesapeake Bay. The second set is comprised of stations with long enough temperature records to generate a climatology and compute the SST anomaly. The analysis from these 51 stations gives an error assessment which is more indicative of expected errors in the MHW calculation. The distributions of each of these two sets of validations is shown in Figure 3, overlaid on top of mean SST from Geo-Polar.

To evaluate the accuracy of the three satellite datasets in measuring SST, the observed temperature from each satellite dataset was compared to in situ observations. All satellites have RMSEs of less than 2°C, with Geo-Polar performing the best and MUR performing the worst. All datasets are also on average biased about 0.5°C cold. (Table 2). In addition to a smaller RMSE Geo-Polar has less variance than MUR. MUR had more outliers, although all datasets underestimate extreme values (Figure 4). All datasets are most accurate in the main stem of the Bay and least accurate closer to shore (Figure 5). Geo-Polar and OSTIA have the largest errors in the upper Potomac and the outflow of the Susquehanna River, while MUR has the largest errors on the western shore rivers north of Baltimore, such as the Gunpowder and Bush Rivers. MUR also generally has higher mean error the Geo-Polar near the Eastern

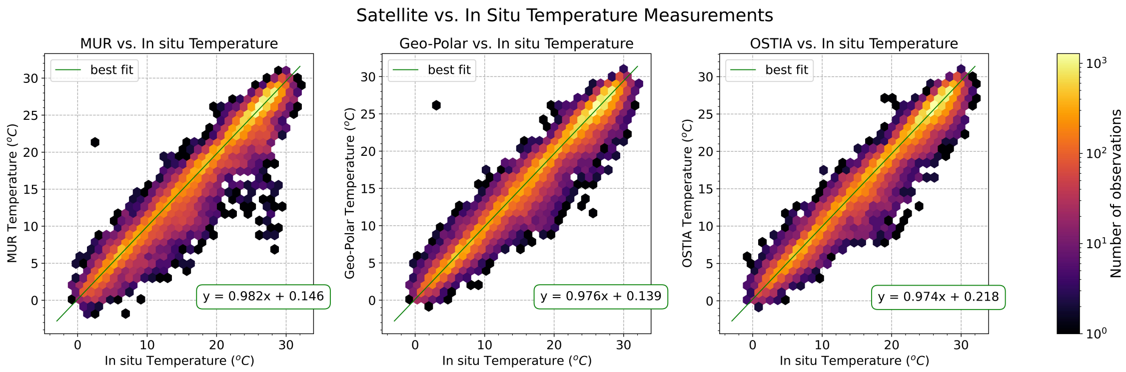

Fig. 4 Density plots of surface temperatures for MUR SST, Geo-Polar SST, and OSTIA SST data products as compared to the Chesapeake Bay Program (CBP) in situ dataset. The left panel shows MUR and the right panel shows Geo-Polar. Green lines on each plot show the linear fit of observations. Geo-Polar has less variance than MUR, while both datasets underestimate extreme values

shore. Overall, Geo-Polar and OSTIA are fairly similar. MUR performs on a similar order of magnitude as the other two datasets, but is slightly less accurate by most metrics.

Two possible reasons for the land edge cooling effect along the shoreline were considered. These coastal errors could be due to the land surface decreasing temperature faster at night when compared to the ocean, biasing down the observations in nearshore pixels. Another factor may be the different diurnal temperature cycles in the main stem of the Bay and the tributaries. The depth averaging process was done to account for the fact that most CBP measurements were taken during the day. This choice may not mitigate the diurnal cycle of daytime warming in the well-mixed tributaries as well as it does in the deeper, less well-mixed main stem of the Bay.

Table 2 Satellite SST Mean Errors

Product Name	Slope	Intercept (°C)	RMSE (°C)	R^2	Mean Bias (°C)
MUR	0.98	0.15	1.81	0.95	-0.52
Geo-Polar Blended	0.98	0.14	1.57	0.97	-0.50
OSTIA	0.97	0.22	1.60	0.96	-0.49

As extreme temperature events, MHWs are deviations from a climatological mean. Because of this, mean error in the daily climatological SST values does not affect the MHW calculation as it is eliminated when subtracting the daily climatological value from the anomaly SST value. What matters instead is whether the temperature anomaly from the daily climatology (i.e. the difference between the observed SST and the daily climatological SST value) is accurate. Here we evaluate the suitability of the satellite SST for analyzing MHWs using the error in the SST anomaly from a daily climatology as opposed to the error in the raw SST value. This method of validation better reflects expected errors in our MHW analysis.

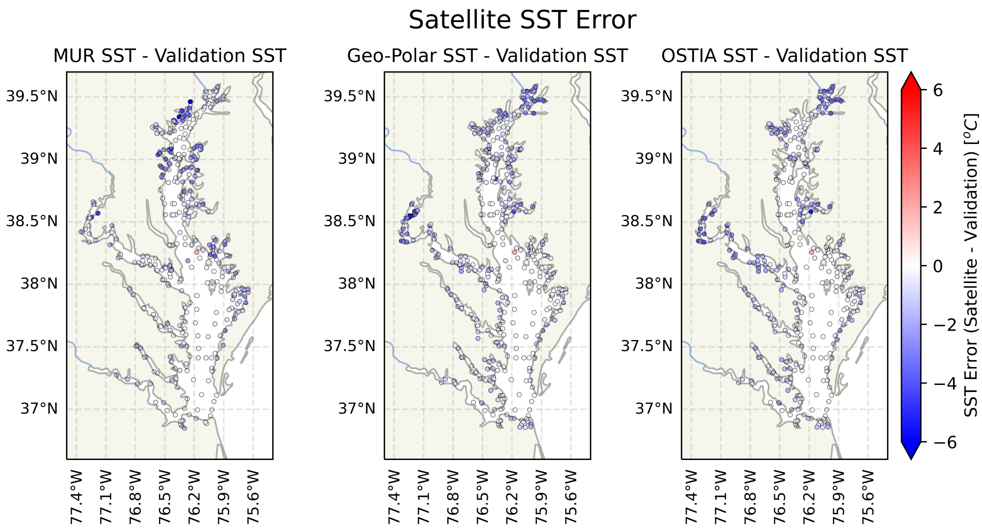

Fig. 5 Spatial distribution of the mean error between the satellite SST datasets and the Chesapeake Bay Program in situ data. Both datasets are most accurate in the main stem of the Bay and have the largest errors near shore. The areas of largest error vary between the two satellites.

To compare the satellite and in situ data, the SST anomalies were computed for observations over the 21 year period. Due to a sparsity of measurements in the in situ data the climatologies were computed on a monthly basis. In situ anomaly SST values were then computed as deviations from the monthly climatology. For most similar comparison of the CBP and satellite datasets a subset of satellite data comprised of days with collocated CBP measurements was used. The same process as used for the CBP data was then used for the satellite dataset. A monthly satellite climatological value was computed using the CBP-collocated subset of observations. The anomaly value was computed by subtracting the observed SST from the monthly climatological value. In situ data was compared with the one collocated satellite pixel from the day of the in situ observation. The original in situ dataset was filtered substantially to achieve this calculation. Of the several hundred stations in the CBP dataset, 51 stations were identified with sufficient temporal coverage to compute a climatological baseline. There is a consistent seasonal sampling bias among the CBP in situ stations, in which summers are more highly sampled than winters (Figure 6). To minimize the impact of this bias on our analysis, stations were vetted by both number of observations and monthly consistency of observations. A station needed to have at least one observation every month in at least 57% of the years (12 of 21 years). Stations were also required to have at least one observation per month in 10 of the 12 months in 86% of the years (18 of 21 years). At the end of this station selection process there remained a seasonal sampling bias, however winter months were still represented.

Figure 6 shows the spatial distribution of the anomaly validation stations. The most important area for our analysis, the main stem of the Bay, is well covered by validation stations, with the exception of one portion of the lower bay. The Potomac

River and Susquehanna outflow are also well covered, as are many of the Eastern shore river outflow regions in the upper and middle bay. The major lower bay rivers, however, including the Rappahannock, the York, and the James, do not have any useable validation stations. We therefore focus our analysis of tributaries primarily on those with validation stations. Validation data is important for assessing the effectiveness of space-borne satellite monitoring for estuaries such as the Chesapeake Bay. Increased in situ observations (which meet the criteria for evaluating MHWs as described above) in the under-sampled areas of the Bay would be valuable to future investigations.

Finally, we evaluated the likelihood that errors in satellite measurements would correlate temporally causing spurious identification of MHWs. To do this we computed the temporal autocorrelation of the error in water temperature anomaly from climatology. The in situ dataset does not provide the temporal resolution to compute autocorrelation with a daily lag, so buoy data from NOAA's Chesapeake Bay Interpretive Buoy System (CBIBS) was used instead. Past work comparing buoy data with satellite data can be found in (Mazzini and Pianca, 2022). We selected 3 buoys, one each in the Upper, Middle, and Lower Bay (Table 3). The Upper Bay buoy only had about 6 years of observations, but was still included for spatial coverage. Only nighttime (12am-7am local time) buoy measurements were used to match the satellite SST foundation temperature definition and missing data in the buoy record was dropped when calculating autocorrelation. The decorrelation timescale was computed and defined as the number of days at which the autocorrelation dropped below e^{-1}.

Table 3 CBIBS Buoy Data Sources

Buoy Name	Section	Approx. Latitude	Approx. Longitude	Operating Years	No. of Days of Observations
Annapolis	Upper	38.96°N	76.45°W	2013-present	2308
Goose's Reef	Middle	38.56°N	76.42°W	2011-present	3107
Stingray Point	Lower	37.57°N	76.26°W	2012-present	3532

2.4 Effects of Satellite SST Errors on Marine Heatwave Calculations

Table 4 Satellite SST Anomaly Mean Errors

Product Name	Slope	Intercept (°C)	RMSE (°C)	R^2	Mean Bias (°C)
MUR	0.86	0.19	1.42	0.53	0.0007
Geo-Polar Blended	0.81	0.01	1.00	0.70	0.0024
OSTIA	0.78	-0.04	1.06	0.67	-0.0995

Using satellite SST in the narrow Chesapeake Bay pushes the limits of these satellite datasets. To understand the potential impact of satellite data on the robustness

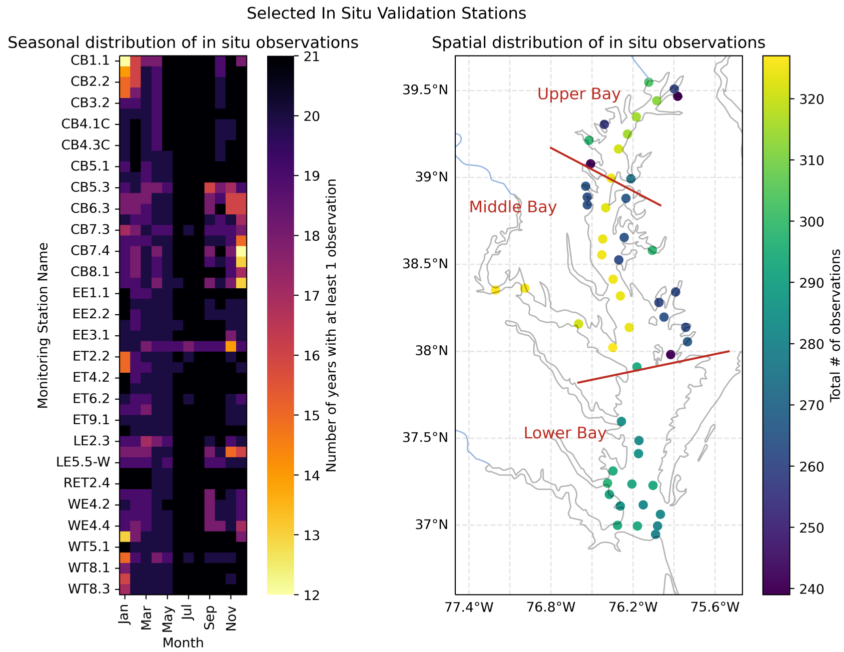

Fig. 6 The left panel shows the monthly distribution of in situ observations for each of the validation stations used. Color shows the number of months in the 21 year time series that had at least one observation. The right plot shows the spatial distribution of validation stations, colored by the total number of observations. Validation stations cover the majority of the main stem of the Bay and several important tributaries. There is a seasonal bias in observations, however winter months are still represented.

of the MHW analysis, we considered the following forms of error: 1) mean error 2) frequency distribution (histogram) of satellite errors 3) temporal autocorrelation of error 4) long term and seasonal variability in satellite errors 5) spatial variability in satellite errors. Not all forms of errors in the satellite SST product, however, will propagate to the MHW calculation in the same way.

To assess the mean error between the satellite and in situ SST anomaly estimates of slope and root mean squared error (RMSE) were used (Table 4). Due to the presence of outliers in this dataset regressions were computed using a robust linear regression with a Tukey Biweight norm. Results from the three satellite datasets were quantitatively similar, with Geo-Polar performing the best in RMSE. The slopes of less than 1 with intercepts close to 0 indicate that both datasets underestimate extreme values, suggesting that our results could be an underestimate of extreme events. All three datasets have very low mean biases, with the largest mean bias being -0.1°C in OSTIA. These relationships and the lower variance of Geo-Polar can also be seen in the distributions of Figure 7. Underestimates in extreme values would result in lower maximum intensities and could also contribute to lower cumulative intensity, rate of onset, and rate of decline. Due to the lower RMSE we chose to calculate MHW using the Geo-Polar Blended SST product. The remainder of our validation results are therefore only shown for Geo-Polar.

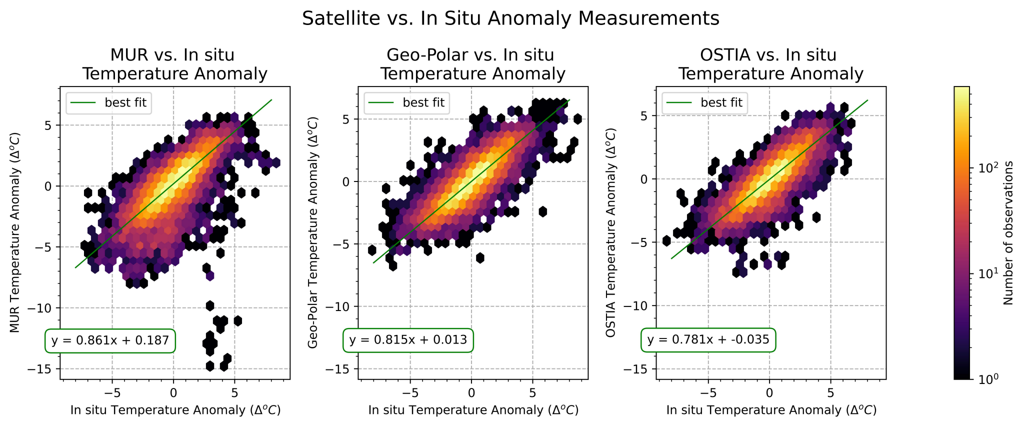

Fig. 7 Density plots of the anomaly error for MUR SST, Geo-Polar SST, and OSTIA SST products as compared to the Chesapeake Bay Program (CBP) in situ dataset. The left panel shows MUR and the right panel shows Geo-Polar. Green lines on each plot show the linear fit of observations. Geo-Polar has a less variance than MUR, while both datasets underestimate extreme values.

For the purposes of MHWs, errors need to be adjacent in time to produce false MHW. To evaluate this we estimate the error decorrelation timescale. For all 3 of the tested buoys the decorrelation timescale was either 3 or 4 days, less than the 5 day minimum length of a MHW. So while the SST mean errors are non negligible they decorrelate on a timescale shorter than the threshold for MHW identification.

Lower-frequency temporal variation is another important form of potential bias in satellite errors. A Hovmöller plot shows there is not consistent seasonality in anomaly errors (Figure 8). Summers, however, do show a long term trend in error from March through August. These months underestimate anomaly values prior to 2011 and overestimate anomaly values in 2011 onward. This increasing long term error could lead to an overestimate in the long term trend in summertime MHW occurrences and intensity, discussed further in section 3.3. Hovmöller plots for all three satellites are available in the supplemental material.

Spatially, the mean error displayed very little variation (Figure 9), indicating that spatial variations in MHW, the focus of this paper, are likely not unduly influenced by satellite errors. In contrast, the long term trend in the error was largest in the upper bay and insignificant in most of the lower bay. Several of the lower bay tributaries, including the Rappahannock, the York, and the James Rivers, did not have any validation stations (Figure 6). Because of this we proceed with caution when interpreting results in these tributaries.

We note the primary caveat in our validation analysis is uncertainty in the approximation of foundation temperature from the in situ data for comparison with satellite SST. While the calculation of foundation temperature in the open ocean is well-established, identifying this depth in the dynamic estuarine setting is more difficult. Some areas of the Bay, for example, are shallow well mixed and no depths are free

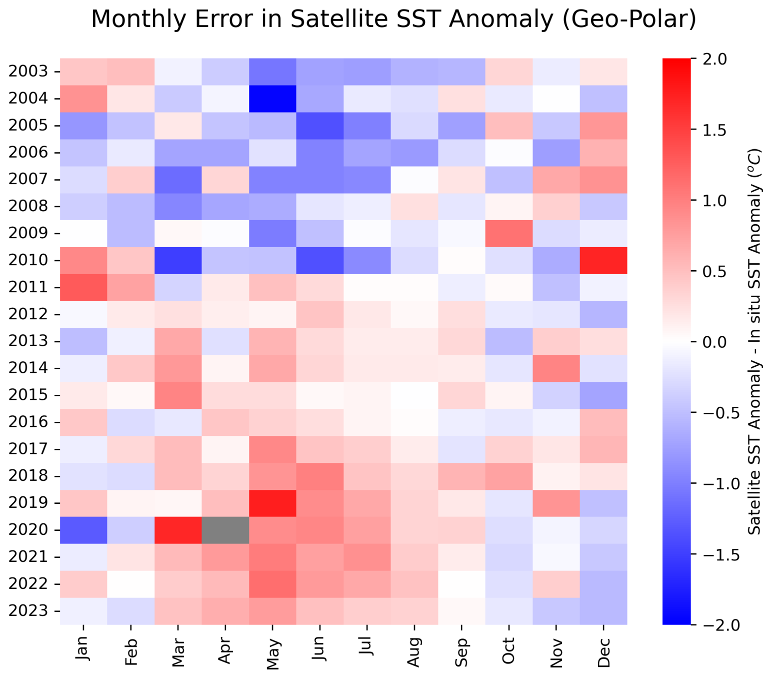

Fig. 8 The error in SST anomalies from climatology for Geo-Polar by month and year. Each pixel corresponds to the average satellite error for all pixels in the Bay during that year (x axis) and month (y axis). The colorbar shows satellite SST minus in situ measurements, such that negative (blue) values represent satellite SST underestimates of in situ temperature anomaly. Geo-Polar SST has a long term trend in the error in SST anomaly from climatology over time in summer months, but no consistent seasonal error.

of diurnal temperature variation. Additionally, in estuaries tidal advection and diurnal variability from the solar heating cycle can be of the same order of magnitude. This makes direct comparison between satellite estimates of foundation temperature and in situ SST measurements less clear and complicates error estimation. Overall, we expect our analysis underestimates the maximum intensity, and may overestimate the strength of long term trends. However, the fast decorrelation timescale of errors relative to the MHW identification threshold is expected to limit the effect of errors on the identified patterns of MHW characteristics. We address the relative magnitudes of these effects in the context of our results in the next section (3).

3 Results

3.1 Temporal Marine Heatwave Characteristics

Many major documented MHW in the Northwest Atlantic Ocean also appear in the Chesapeake Bay, including MHWs in summer 2012 (Mills et al, 2013), winter 2015-2016/fall 2016 (Pershing et al, 2018), and early spring 2017 (Gawarkiewicz et al, 2019). One MHW of particular interest for the Bay was a September 2005 heatwave, during

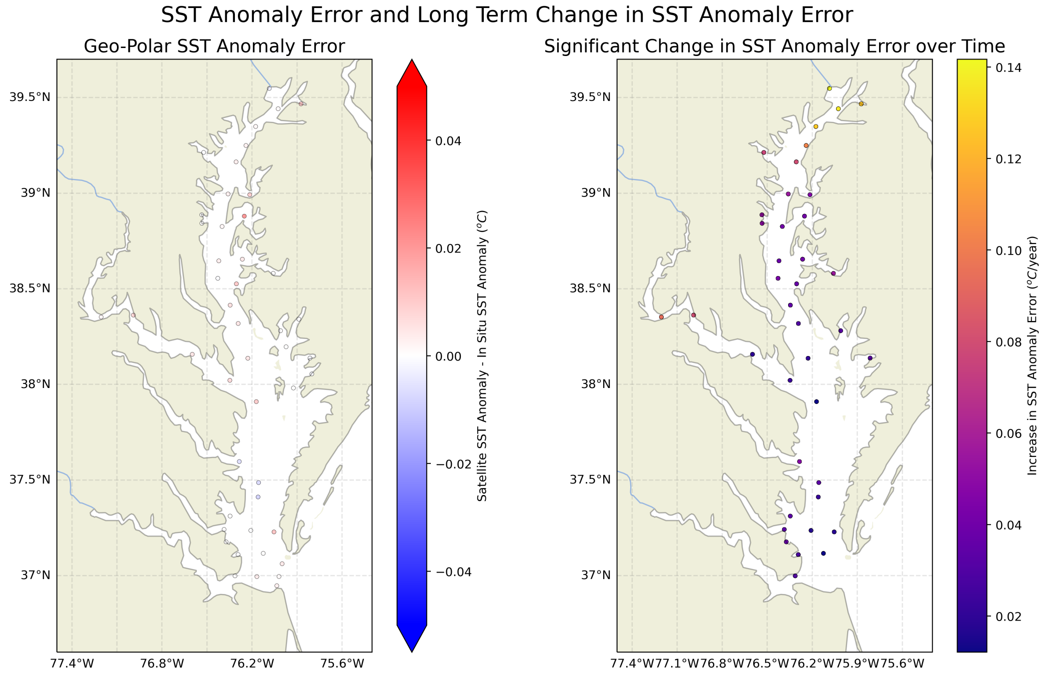

Fig. 9 Maps display the spatial distribution of error across the validation stations. The left figure shows the mean error. The right figure shows the long term trend in the error. Only stations with a significant trend are displayed (p value less than 0.05). Mean error is consistent throughout the Bay, but long term trend in error shows a north/south gradient, discussed further in section 3.3.

which anomalously high temperatures were shown to decrease commercially relevant seagrass habitat (Smith et al, 2023). The evolution of this MHW is shown in Figure 10 as an example of the capabilities of the satellite data and to contextualize the aggregate statistics presented later. The MHW first emerged in the center of the Bay, expanded to encompass most of the main stem by the peak, then receeded beginning in the upper Bay. The last area to experience high temperatures was the mouth of the Bay. The strongest anomalies were in the upper bay near Baltimore. While this MHW affected the full Bay and decayed toward the Bay mouth, other MHW show different patterns of spatial evolution. For example, some MHW begin in the river outflow regions. Additional work could consider these different spatial patterns of evolution and decline, as they may give insight into different driving mechanisms.

The frequency of MHW in the Chesapeake Bay is increasing over time (Mazzini and Pianca, 2022), consistent with the global trend (Oliver et al, 2018). Figure 11 shows the number of annual MHW events over time in the upper, middle, and lower sections of the Bay. All SST pixels over each of the three sections were averaged together to generate a single annual result. The results from our analysis are shown alongside results from Mazzini and Pianca (2022), which derive MHW frequency from buoy data. There is good agreement between the buoy-derived MHW frequency and the

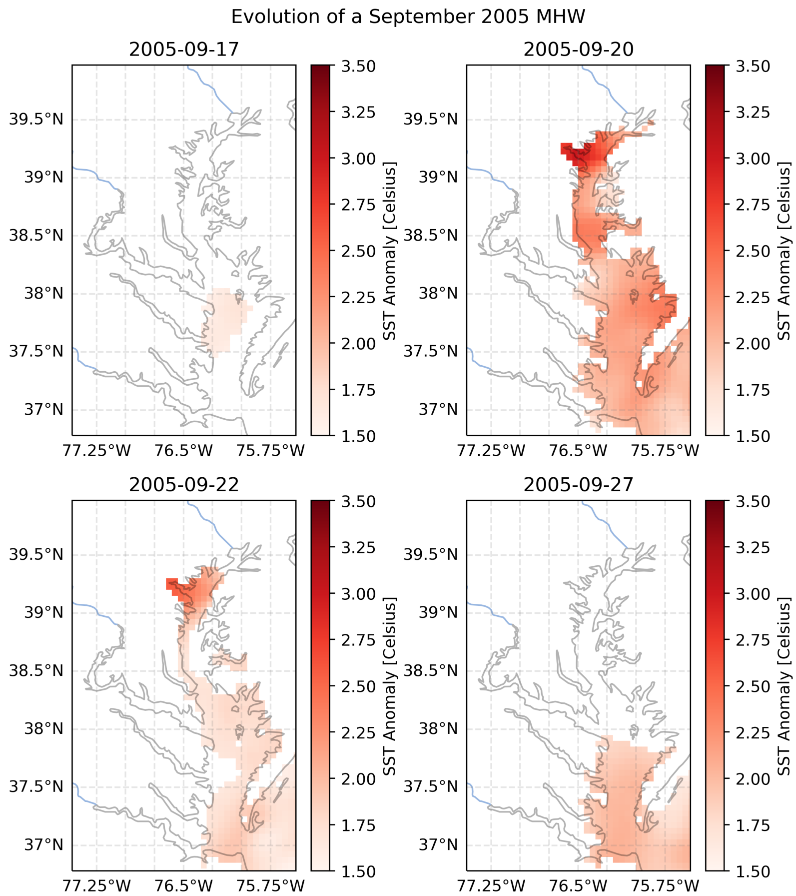

Fig. 10 Evolution of temperature anomaly during a 2005 MHW. The 4 panels show 4 dates throughout the MHW: September 17th, September 20th, September 22nd, and September 27th. Only pixels with an identified MHW are plotted.

satellite-derived MHW frequency. Mazzini and Pianca (2022) found that there were on average 2 MHW per year with an average duration of 11 days per year, resulting in an average of 22 MHW days per year. The satellite derived MHW produce consistent results, with a bay-wide average of 2.3 MHW per year and 10.8 days / MHW for a total of 25 MHW days per year. Comparison of these results with Mazzini and Pianca (2022) provides a further form of validation of our approach.

Because MHW are defined relative to a daily climatological baseline, MHW can occur at any time of the year. Figure 12 shows monthly aggregations of MHW for the 6 MHW characteristics. Each MHW in the dataset is counted once and grouped into the month in which it started. Errors in the medians are computing using 2000 iterations of bootsrapping. In the Chesapeake Bay, there is statistically significant seasonality in all six characteristics with an approximate doubling between the minimum and maximum values of each characteristic. MHWs are most prevalent in the Summer with a

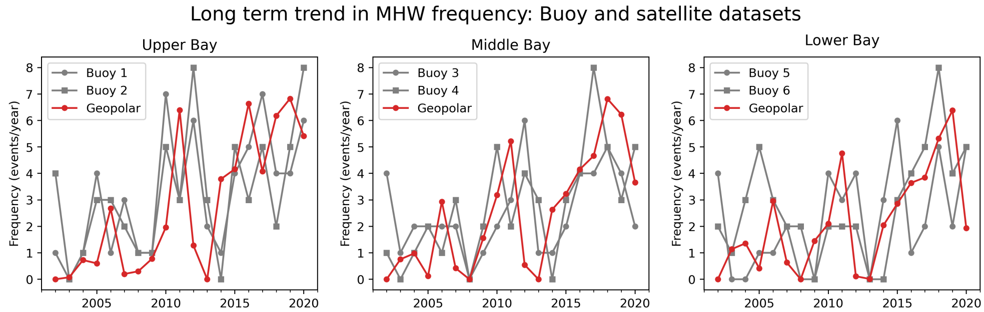

Fig. 11 Time series of MHW frequency in the upper, middle, and lower sections of the Chesapeake Bay. (See Figure 6 for Bay regions). Frequency of MHW is increasing in all three regions of the Bay. Frequency calculated using Geo-Polar SST, plotted in red, is shown alongside MHW frequency derived from buoys, plotted in gray. Buoy-derived MHW frequency was reported in Mazzini and Pianca (2022). Regional MHW frequencies are consistent between Geo-Polar and buoy-derived MHW characteristics.

secondary spike in January. Mazzini and Pianca (2022) also found a summertime peak in MHW, however because Mazzini and Pianca (2022) aggregate by season instead of month it is not clear if their buoy-based analysis also showed a January spike. MHW duration has an inverse relationship to the number of MHWs, with duration peaks in March and December. MHW that begin in December and March have durations that are highly variable, as opposed to summer MHW which have more consistent durations. Maximum and cumulative intensity follow the duration pattern, indicating that MHW that begin in March or December are the longest lasting and have high maximum intensities. A subsurface MHW study by Shunk et al (2024) found that MHW in the Chesapeake Bay follow two regimes: a spring-summer regime where temperature anomalies are confined to the mixed layer and a fall-winter regime that is more vertically homogeneous. The satellite observed seasonality in duration, with longest MHW in the winter, could be related to the presence of temperature anomalies throughout the water column and slower rates of decline due to the larger volume of water experiencing anomalies. Rates of onset and decline both have peaks in the Spring and Fall, although they differ in that rate of onset remains high in January/February while rate of decline decreases in this same period. The overall variation is large - with all characteristics experiencing at least a doubling between the minimum and maximum months.

The bay-wide average of about 25 MHW days per year is overall spatially uniform (Figure 13). Considering only MHW days, however, obscures significant spatial variability in the duration and frequency of MHWs in the Bay. Average number of annual MHW and MHW duration show a north-south gradient, ranging from about 2-3 MHW per year and MHW durations between 8 and 13 days. The average number of annual MHW is highest in the northern areas of the Bay while the average MHW duration is highest is the southernmost regions of the Bay. The counteracting north-south gradients of these two fields leads to the uniform pattern of MHW days. To summarize, over the last 21 years in the Chesapeake Bay longer, less frequent heatwaves are found

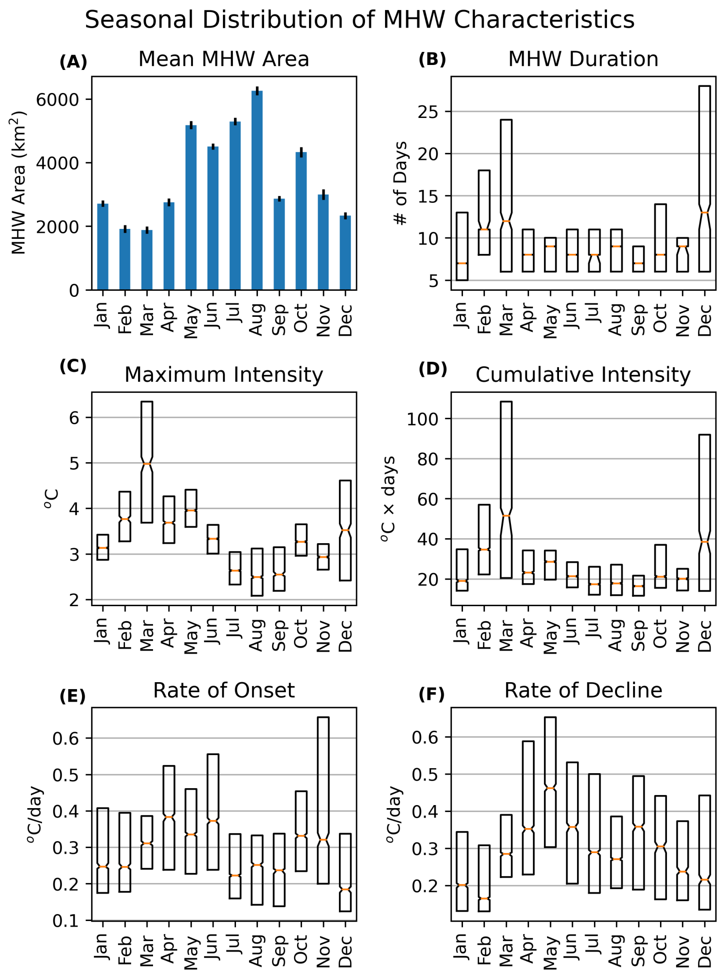

Fig. 12 Monthly distributions of six MHW characteristics defined as shown in Figure 2: (A) the mean area experiencing a MHW with error bars (B) MHW duration (C) maximum intensity (D) cumulative intensity (E) rate of onset (F) rate of decline. Panels (B)-(F) each show the 25th, 50th, and 75th percentile values in the box plots. The error, computed using 2000 iterations of bootstrapping, is represented by a notch in the box plot. The error bars in panel (A) are computed using the standard error of the mean. Each MHW is counted in the month in which it started. There is clear seasonality all of the characteristics, with an approximate doubling between maximum and minimum monthly values.

in the southern regions of the Bay while shorter, more frequent MHW characterize the northern regions. Spatial patterns such as this one are not evident when viewing averaged quantities, as the overall number of MHWs days does not vary significantly across the Bay. In the following section we direct our focus to further consideration of spatial variability in MHW characteristics.

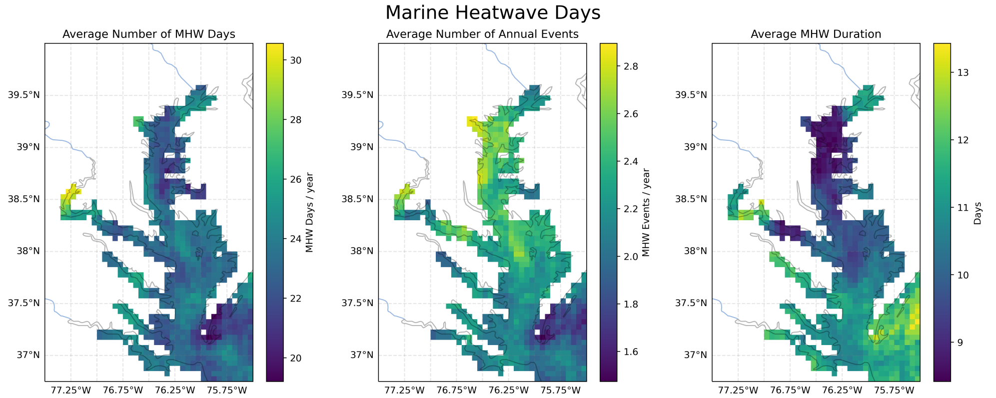

Fig. 13 The spatial distribution of the average number of MHW days per year using Geo-Polar SST. The average number of MHW days is calculated by multiplying the average number per year by the average duration.

3.2 Marine Heatwave Characterization

Satellite observations give a finer grained look at the development and spatial structure of MHWs. This information can suggest physical mechanisms behind MHW development or decay or provide higher resolution insights for resource managers. Here we look at spatial variability in 6 MHW characteristics, each of which indicates something different about the evolution or potential impact of the MHW. The 6 characteristics are: 1) Average number of annual events 2) Average MHW duration 3) Average maximum intensity 4) Average cumulative intensity 5) Average rate of onset 6) Average rate of decline. The first two characteristics are shown in Figure 13 and the remaining 4 characteristics are shown in Figure 14.

MHW characteristics were aggregated to produce maps showing the average value for each characteristic across the full 21 year time series. The end result is 6 maps, one for each of the aggregated MHW characteristics across the Bay. In addition to the 6 aggregated characteristics in the diagram, average intensity was considered, but was found to closely follow patterns in the maximum intensity and therefore is not shown here.

The dominant pattern of spatial variation in MHW characteristics is a north-south gradient in the number of events and duration, as discussed in section 3.1. This north-south pattern is also evident in cumulative intensity. Cumulative intensity is a reflection of two aspects of a heatwave: duration and intensity. A MHW can have high cumulative intensity either because the MHW has a long duration, it has high maximum intensity, or both. In the Chesapeake Bay, MHW cumulative intensity is largest near the mouth of the Bay and minimum in the upper bay, suggesting it is more strongly influenced by duration than by maximum intensity (Figure 14). Average MHW duration doubles between the lowest and highest values in the Bay, while average maximum intensity changes by only a factor of about 1.3. One deviation from the overall north-south gradient is the estuarine turbidity maximum (ETM) just

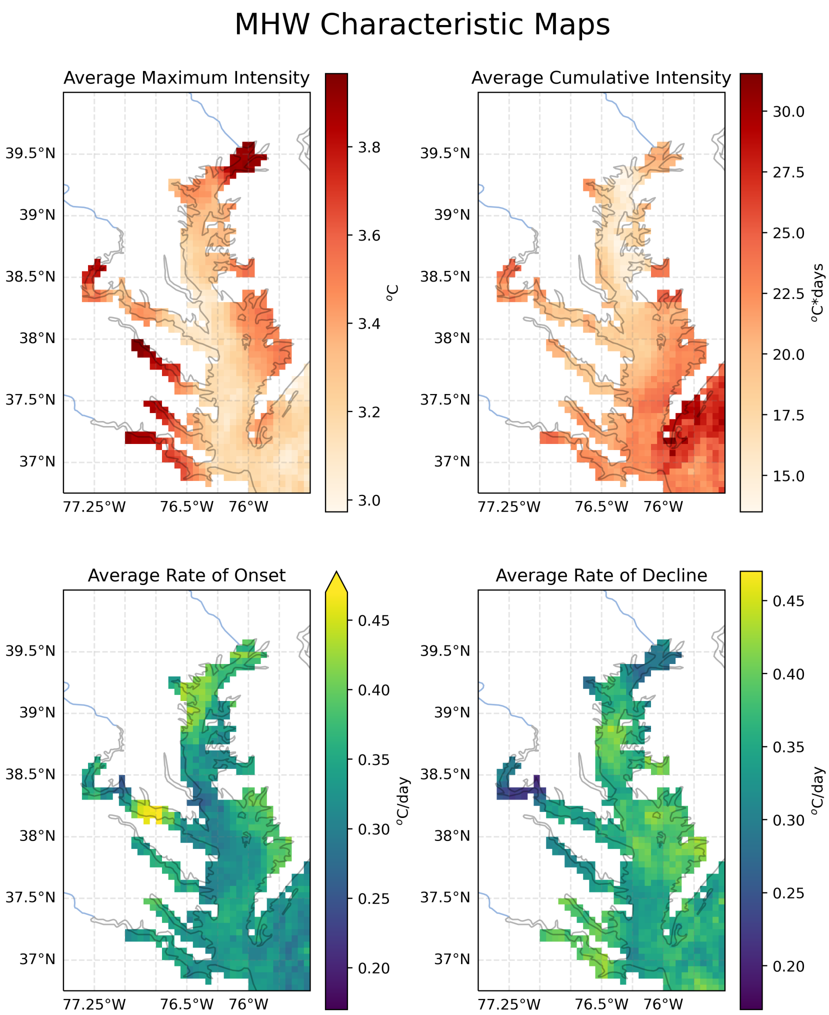

Fig. 14 Spatial maps showing the distribution of 4 MHW characteristics. Maps show an aggregation (either sum or average) of across time for each pixel.

north of Baltimore. The ETM is a region of increased turbidity where salty ocean water collides and mixes with fresh river outflow. The ETM can be seen distinctly in 5 of the 6 MHW characteristics, including in characteristics that do not have a north-south gradient (maximum intensity and rate of decline).

Because maximum intensity is the maximum temperature anomaly relative to the daily climatological baseline, high maximum intensities could be a result of larger standard deviation in temperature values in a particular section of the Bay. The high maximum intensity could also be related to depth, as the shallower water may heat more effectively during a MHW, however we did not find depth to be strongly correlated to MHW intensity (see supplemental material). Past work has shown that low-land rivers are extremely sensitive to air temperature (Piccolroaz et al, 2018), a common driver of marine heatwaves.

Rate of onset and decline are two particularly important characteristics for understanding mechanisms of MHW development and decline. Rate of onset showed an approximately 1.5-fold difference between the highest and lowest values in the Bay(Figure 14). MHW develop the quickest in the upper Bay where temperature anomalies can increase at almost 0.5°C per day. Relative to rate of onset, rate of decline is more uniform in the main stem of the bay (approximately 0.4°C/day). Shunk et al (2024) found that air-estuary heat flux changes, primarily from latent heat, is the leading driver of MHW onset and decline in the Chesapeake. However, the spatial variability in rates of onset and decline in the satellite data may suggest an additional role for other processes in the development and decay of MHW in the main stem of the Bay. Further investigation into the finer scale spatial structure of the rates of onset and decline could be an avenue of future research into drivers of MHW in the Bay.

3.3 Long Term Marine Heatwave Trends

Our analysis of long term trends (see section 2.2) suggests that almost the entire Bay is experiencing significant increases in the number of annual MHW events (Figure 15). The largest values are close to an increase of about 5 additional MHW events per decade, or an approximately 10% increase in number of annual MHW events over the period of 2003-2022. There is significant spatial variation, seen in the factor of 3 difference between the highest and lowest rates of increase in annual MHW events. The upper Bay, which experiences the most frequent but shortest MHW, is also the area that has the greatest increases in number of MHW. The only section of the Bay that does not see significant increases in number of events is the mouth of the Bay. In contrast, average duration and cumulative intensity did not show statistically significant increases over this time period. Given that cumulative intensity structure was controlled by duration we would expect that these two would show a similar trend, or lack thereof. In summary, we are seeing that for most of the main stem of the Bay, the qualitative character of MHWs are not changing, as MHWs are not longer nor are they more intense, but there are more MHWs occurring. This extends the findings of Mazzini and Pianca (2022), who found increases in frequency but no trend in duration at several moorings in the Bay over their study period, 1986-2020.

The error analysis in section 2.4 revealed a spatial trend in the long term error with spatial variation in the error of the long term trend having a pattern that mirrors the observed trend in number of MHW: largest in the upper Bay and decreasing to the south. However, average increase in SST anomaly error in the upper Bay is 0.1°C/year (Figure 9). The upper Bay in the upper right panel of figure 15 shows an increase of about 2.4°C per decade, implying there is at least a 1.4°C per decade increase in MHW intensity in this portion of the Bay. The relative magnitudes of error and signal give confidence in the results.

While a large body of MHW literature has centered on the definition of a MHW with a fixed climatological baseline described in Hobday et al (2016), there is a growing body of work utilizing a detrended SST for the climatological baseline (ex. Jacox et al, 2020). These two approaches provide different insights into future change and resource

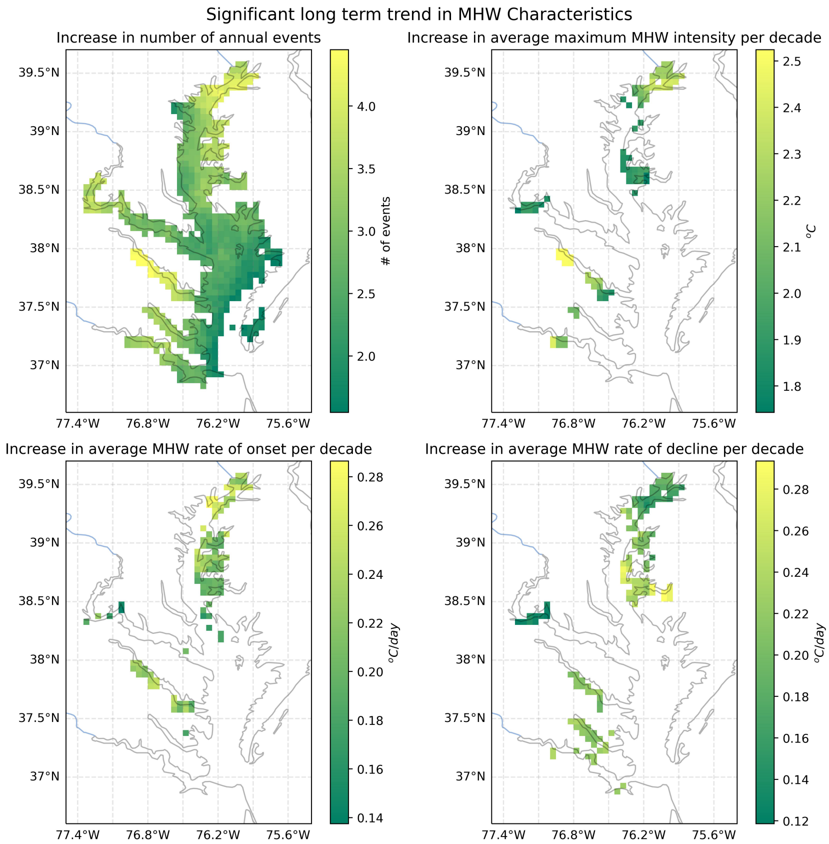

Fig. 15 Long term trends in MHW characteristics. Plots show the slope of a linear regression on each pixel in increases per decade. Only those pixels considered statistically significant under multiple hypothesis testing with a false discovery rate of 10% were included.

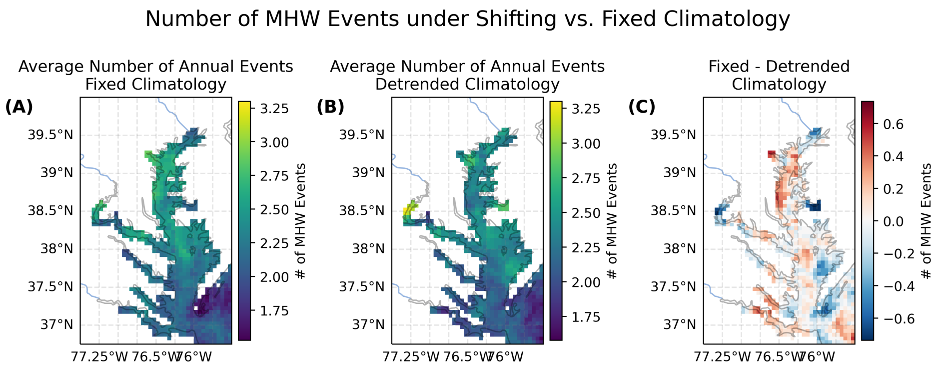

Fig. 16 Aggregated maps showing the average number of annual MHW events using (A) unmodified SST and (B) detrended SST. Panel (C) shows the difference of the two. Red zones in panel (C) show where MHWs are attributable to long term warming. We see strong influence of long term warming on the number of annual MHW events in the upper Chesapeake Bay.

management (Amaya et al, 2023). Here we calculate annual number of MHW events with a detrended SST to highlight which aspects of the spatial pattern are related to long term warming as opposed to changes in extreme events. The differences between the fixed and detrended climatologies suggest that the processes that generate MHW in these locations are attributable to long term warming. This is the case for much of the upper Bay and is shown in red in Figure 16, Panel C. This decrease in MHW events in the upper Bay is also seen in the weaker north/south gradient in the detrended MHW analysis.

These data suggest that changes in MHW in the Chesapeake are not due to changes in spread of temperatures, or an increase in extreme values, but rather due to changes in the mean temperature. There are no significant long term trends in any MHW characteristic when computing MHW characteristics using the detrended climatology, evidence that increases are due to changes in the mean temperature. Past work has also attributed MHW trends to a long term change instead of increases in extreme temperature values (Mazzini and Pianca, 2022).

4 Discussion

Estuarine environments provide critical ecological and economic value, however studies of estuarine marine heatwaves have been scarce. Availability of monitoring data is a common limitation, and buoy data does not provide highly resolved spatial structure, which can limit understanding of impacts and drivers. Here we used satellite data to provide a novel, spatially resolved picture of MHW in the Chesapeake Bay.

Three satellite SST sources, NASA MUR, NOAA Geo-Polar, and Copernicus Marine OSTIA, were evaluated against in situ measurements. All datasets likely underestimate extreme values and over estimate summertime long term trends, but show spatial consistency in SST anomalies. Validation work such as this is critical for accurate interpretation of global SST datasets in coastal zones. This validation was possible because of the availability of in situ validation data, but this resource is not as widely available in every estuary. While estuaries differ in dynamic conditions and seasonal variability, successful use of satellite SST in the Chesapeake suggests that the application of satellite SST for spatially-resolved temperature studies in other large estuaries may be possible. Use of well-calibrated regional models may provide an alternate method for validating the use of satellite data in estuaries where there is otherwise insufficient in situ data.

MHW characteristic maps reveal spatial variation in the Chesapeake, where the dominant pattern of variability is a north to south (along estuary) gradient. Spatial structure reveals that cumulative intensity is dominated by MHW duration, not max intensity. This result, coupled with the strong bay wide variation in MHW duration, highlight MHW duration as a key MHW characteristic in the Chesapeake Bay. Temporal MHW analyses show increases in MHW frequency over time and an average of 25 MHW days per year bay-wide. Increases in MHW events in the lower Bay result in approximately 5 additional annual events per decade, a near doubling of MHW frequency over the 21 year satellite period. Comparison of these results with a detrended SST analysis suggest that long term warming influence on MHW characteristics is particularly influential in zones of river influence. Confidence in long term trends is tempered by changes in satellite error over time, pointing to the criticality of periodic reanalyses of satellite data to identify and correct for systematic error. Satellite-derived MHW analysis is consistent with past buoy based analysis from Mazzini and Pianca (2022), giving confidence in the accuracy of this new technique. Given that the satellite data likely represents an underestimate of temperature (Section 2.4), it is possible these trends are even stronger. Increased spatial resolution and clarity into regional trends in MHW characteristics benefits our understanding of extreme temperature events in the Chesapeake Bay and could benefit monitoring efforts that help mitigate the high economic impact and conserve protected waters.

The success of the satellite technique for analyzing MHW in rivers is not clear. In the lower tributaries of the Bay (the Rappahannock, York, or James rivers) we are limited by a lack of long term monitoring stations in the river tributaries to provide validation data. There are some available validation stations in the Potomac and Susquehanna outflow region, however the performance of the satellite data in these regions remains poor, with mean SST errors of 3-4° Celsius. These tributary regions are critical areas for resource managers and further improvement or algorithmic development focusing on these regions would be of scientific and public benefit. The difficulty of this highlights the need for long term monitoring stations, especially in tributaries.

While our results show that increasing MHW are due to long term warming, past work investigating long term warming in the Chesapeake Bay show that surface warming is overall spatially consistent, with only slightly faster warming at the mouth of the Bay (Hinson et al, 2022). The spatial variability seen in this work implies that, while the largest contribution to MHW increase may be long term warming, there are still additional characteristics, or causes, of MHW that may be changing over time. More detailed investigation into the dynamical drivers of MHW will be needed to identify why there is a lack of spatial variability in long term warming but spatial variability in MHW frequency increases.

Global MHW work has found that large scale atmospheric pressure anomalies are a driver for MHW in the mid and high latitudes (Holbrook et al, 2019). Tassone et al (2022) looked at estuarine MHW in particular, finding that in the Chesapeake Bay atmospheric and oceanic MHW were co-occurring over 50% of the time, the second highest co-occurrence of the 12 estuaries studied across the United States. The Chesapeake Bay, however, had only the sixth most number of events, highlighting the variability of MHW behavior between estuarine environments. These findings agree with those of Shunk et al (2024), which found changes in air-estuary heat flux to be the primary driver of MHW onset and decline. While atmospheric MHW likely play a strong influence in generating MHW in the Chesapeake Bay Tassone et al (2022) also found that oceanic MHW tended to lag atmospheric MHW in the Chesapeake Bay by only 1 day, and highlight that in some cases a relatively low intensity, low duration atmospheric MHW are enough to push an estuarine environment into a MHW when water temperatures are already elevated.

Future analysis could focus on connecting spatial patterns of MHW characteristics identified here to MHW mechanisms of development and decline in the Chesapeake.

Patterns of evolution, such as the example in Figure 10, hint at multiple spatial patterns of evolution that could indicate differing influences. For example, some MHW appeared to develop starting in the river tributaries and expand to the main stem, while others appeared to begin at the mouth of the Bay, perhaps reflecting the relative influence of rivers and the coastal ocean. Another avenue could be to pursue the spatial patterns in rates of onset and decline. Past work in the North Atlantic suggests atmospheric mechanisms to be the most influential mechanism in MHW development while ocean processes to be the more influential mechanism in MHW decline (Schlegel et al, 2021). Rate of onset and decline in the Chesapeake Bay showed the finest scale spatial structure of the metrics considered here, and differences in their distributions could be related to mechanistic influence.

The Chesapeake Bay is the largest estuary in the continental US and the impacts of a warming climate have societal and economic impact. This work provides a spatial analysis of MHW characteristics and trends in the Chesapeake. Validation of satellite SST in the Bay allows future researchers to more accurately understand results derived using SST in the Bay. Spatial variation in MHW characteristics highlights the importance of spatial structure in the Bay, highlights the differences between river regions and main stem waters, and provides initial insight into possible MHW mechanisms.

5 Declarations

5.1 Funding

This study was supported by NOAA grant NA19NES4320002 (Cooperative Institute for Satellite Earth System Studies-CISESS) at the University of Maryland/ESSIC. Jacob Wenegrat acknowledges support from NSF award 2126474. The scientific results and conclusions, as well as any views or opinions expressed herein, are those of the author(s) and do not necessarily reflect the views of NOAA or the Department of Commerce.

5.2 Competing Interests

The authors certify that they have no affiliations with or involvement in any organization or entity with any financial interest or non-financial interest in the subject matter or materials discussed in this manuscript.

5.3 Code Availability

The code associated with the article can be accessed via Github: https://github.com/rwegener2/chesapeake_mhw

The authors would like to acknowledge that this work would not have been possible without the contributions of many open source software libraries, including pandas (pandas development team, 2020), xarray (Hoyer and Hamman, 2017), project jupyter (Kluyver et al, 2016), scipy (Virtanen et al, 2020), dask (Dask Development Team, 2016), matplotlib (Hunter, 2007) and cartopy (Met Office, 2010 - 2015).

5.4 Data Availability

Processed data used to generate all figures has been submitted to the Sea Scientific Open Data Publication (SEANOE) (reference number 105013). This includes:

1. SST values for Chesapeake Bay Program data and each of the satellite datasets at each of the dates and locations used (csv file format). Used to generate figures 4 and 5.
2. SST anomaly values for Chesapeake Bay Program data and each of the satellite datasets at each of the dates and locations used (csv file format). Used to generate figures 7, 8, and 9.
3. Average MHW characteristics for each pixel based on Geo-Polar SST (netcdf file format). Used to generate figures 13, 14, 15, and 16.

Raw SST data from NOAA Geo-Polar, NASA MUR, Copernicus Marine OISTA, and the Chesapeake Data Program has also been submitted to SEANOE for ease of replication. Satellite datasets (Geo-Polar, MUR, and OSTIA) have been subset to the Chesapeake Bay region and study time frame and are available in the netcdf file format. Unprocessed Geo-Polar SST was used to generate figure 10. Chesapeake Bay Program in situ water temperature measurements for the Chesapeake Bay and study time frame were also submitted to the SEANOE repository (csv format).

5.5 Author Contribution

Rachel Wegener: Conceptualization, Methodology, Software, Investigation, Data curation, Writing - Original Draft, Visualization. Jacob Wenegrat: Conceptualization, Methodology, Writing - Review & Editing, Supervision, Project administration. Veronica P. Lance: Conceptualization, Methodology, Writing - Review & Editing, Supervision, Funding acquisition. Skylar Lama: Software, Formal analysis, Data curation. The scientific results and conclusions, as well as any views or opinions expressed herein, are those of the author(s) and do not necessarily reflect the views of NOAA or the Department of Commerce.

References

Amaya DJ, Jacox MG, Fewings MR, et al (2023) Marine heatwaves need clear definitions so coastal communities can adapt. Nature 616(7955):29–32. https://doi.org/10.1038/d41586-023-00924-2

Batiuk R, Brownson K, Dennison W, et al (2023) Rising watershed and bay water temperatures: Ecological implications and management responses – a stac workshop. STAC Publication Number 23-001 URL https://www.chesapeake.org/stac/wp-content/uploads/2023/01/FINAL_STAC-Report-Rising-Temps_April.pdf

Bilkovic DM, Mitchell MM, Havens KJ, et al (2019) Chapter 15 - chesapeake bay. In: Sheppard C (ed) World Seas: an Environmental Evaluation (Second Edition). Academic Press, p 379–404, https://doi.org/10.1016/B978-0-12-805068-2.00019-X

Chatterjee A, Anil G, Shenoy LR (2022) Marine heatwaves in the arabian sea. Ocean Science 18(3):639–657. https://doi.org/10.5194/os-18-639-2022

Chesapeake Bay Program (2020) Water quality datahub. URL https://datahub.chesapeakebay.net/WaterQuality

Chin TM, Vazquez-Cuervo J, Armstrong EM (2017) A multi-scale high-resolution analysis of global sea surface temperature. Remote Sensing of Environment 200:154–169. https://doi.org/10.1016/j.rse.2017.07.029

Dask Development Team (2016) Dask: Library for dynamic task scheduling. URL http://dask.pydata.org

Ding H, Elmore AJ (2015) Spatio-temporal patterns in water surface temperature from landsat time series data in the chesapeake bay, u.s.a. 168:335–348. https://doi.org/10.1016/j.rse.2015.07.009

Donlon C, Robinson I, Casey KS, et al (2007) The global ocean data assimilation experiment high-resolution sea surface temperature pilot project. Bulletin of the American Meteorological Society 88(8):1197 – 1214. https://doi.org/10.1175/BAMS-88-8-1197

Donlon CJ, Martin M, Stark J, et al (2012) The operational sea surface temperature and sea ice analysis (ostia) system. Remote Sensing of Environment 116:140–158. https://doi.org/https://doi.org/10.1016/j.rse.2010.10.017, advanced Along Track Scanning Radiometer(AATSR) Special Issue

Du J, Shen J, Park K, et al (2018) Worsened physical condition due to climate change contributes to the increasing hypoxia in chesapeake bay. Science of The Total Environment 630:707–717. https://doi.org/10.1016/j.scitotenv.2018.02.265

E.U. Copernicus Marine Service Information (CMEMS) (2023) Global ocean ostia sea surface temperature and sea ice analysis. https://doi.org/10.48670/moi-00165

Gawarkiewicz G, Chen K, Forsyth J, et al (2019) Characteristics of an advective marine heatwave in the middle atlantic bight in early 2017. Frontiers in Marine Science 6. https://doi.org/10.3389/fmars.2019.00712

Hinson KE, Friedrichs MA, St-Laurent P, et al (2022) Extent and causes of chesapeake bay warming. J American Water Resour Assoc 58(6):805–825. https://doi.org/10.1111/1752-1688.12916

Hobday AJ, Alexander LV, Perkins SE, et al (2016) A hierarchical approach to defining marine heatwaves. Progress in Oceanography 141:227–238. https://doi.org/10.1016/j.pocean.2015.12.014

Holbrook NJ, Scannell HA, Sen Gupta A, et al (2019) A global assessment of marine heatwaves and their drivers. Nature Communications 10:2624. https://doi.org/10.1038/s41467-019-10206-z

Hoyer S, Hamman J (2017) xarray: N-D labeled arrays and datasets in Python. Journal of Open Research Software 5(1). https://doi.org/10.5334/jors.148, URL https://doi.org/10.5334/jors.148

Huang Z, Feng M, Beggs H, et al (2021) High-resolution marine heatwave mapping in australasian waters using himawari-8 sst and sstaars data. Remote Sensing of Environment 267:112742. https://doi.org/https://doi.org/10.1016/j.rse.2021.112742

Hunter JD (2007) Matplotlib: A 2d graphics environment. Computing in Science & Engineering 9(3):90–95. https://doi.org/10.1109/MCSE.2007.55

Jacox MG, Alexander MA, Bograd SJ, et al (2020) Thermal displacement by marine heatwaves. Nature 584(7819):82–86. https://doi.org/10.1038/s41586-020-2534-z

Kluyver T, Ragan-Kelley B, Pérez F, et al (2016) Jupyter notebooks - a publishing format for reproducible computational workflows. In: Loizides F, Scmidt B (eds) Positioning and Power in Academic Publishing: Players, Agents and Agendas. IOS Press, Netherlands, pp 87–90, URL https://eprints.soton.ac.uk/403913/

Lefcheck JS, Wilcox DJ, Murphy RR, et al (2017) Multiple stressors threaten the imperiled coastal foundation species eelgrass (zostera marina) in chesapeake bay, USA. Global Change Biology 23(9):3474–3483. https://doi.org/10.1111/gcb.13623

Marin M, Feng M, Phillips HE, et al (2021) A global, multiproduct analysis of coastal marine heatwaves: Distribution, characteristics, and long-term trends. Journal of Geophysical Research: Oceans 126(2):e2020JC016708. https://doi.org/10.1029/2020JC016708

Maturi E, Harris A, Mittaz J, et al (2017) A new high-resolution sea surface temperature blended analysis. Bulletin of the American Meteorological Society 98(5):1015–1026. https://doi.org/10.1175/BAMS-D-15-00002.1

Mazzini P, Pianca C (2022) Marine heatwaves in the chesapeake bay. Frontiers in Marine Science 8. https://doi.org/10.3389/fmars.2021.750265

Met Office (2010 - 2015) Cartopy: a cartographic python library with a Matplotlib interface. Exeter, Devon, URL https://scitools.org.uk/cartopy

Mills KE, Pershing AJ, Brown CJ, et al (2013) Fisheries management in a changing climate: Lessons from the 2012 ocean heat wave in the northwest atlantic. Oceanography 26(2):191–195. https://doi.org/10.5670/oceanog.2013.27

Mohamed B, Nilsen F, Skogseth R (2022) Marine heatwaves characteristics in the barents sea based on high resolution satellite data (1982–2020). Frontiers in Marine Science 9. https://doi.org/10.3389/fmars.2022.821646

Oliver E (2023) marineheatwaves. https://github.com/ecjoliver/marineHeatWaves

Oliver ECJ, Donat MG, Burrows MT, et al (2018) Longer and more frequent marine heatwaves over the past century. Nature Communications 9(1):1324. https://doi.org/10.1038/s41467-018-03732-9

Oliver ECJ, Burrows MT, Donat MG, et al (2019) Projected marine heatwaves in the 21st century and the potential for ecological impact. Frontiers in Marine Science 6. https://doi.org/10.3389/fmars.2019.00734

Pershing AJ, Mills KE, Dayton AM, et al (2018) Evidence for adaptation from the 2016 marine heatwave in the northwest atlantic ocean. Oceanography 31(2):152–161. https://doi.org/10.5670/oceanog.2018.213

Piccolroaz S, Toffolon M, Robinson CT, et al (2018) Exploring and Quantifying River Thermal Response to Heatwaves. Water 10(8):1098. https://doi.org/10.3390/w10081098

Schlegel RW, Oliver ECJ, Hobday AJ, et al (2019) Detecting marine heatwaves with sub-optimal data. Front Mar Sci 6:737. https://doi.org/10.3389/fmars.2019.00737

Schlegel RW, Oliver ECJ, Chen K (2021) Drivers of marine heatwaves in the northwest atlantic: The role of air–sea interaction during onset and decline. Frontiers in Marine Science 8. https://doi.org/10.3389/fmars.2021.627970

Shunk NP, Mazzini PLF, Walter RK (2024) Impacts of marine heatwaves on subsurface temperatures and dissolved oxygen in the chesapeake bay. Journal of Geophysical Research: Oceans 129(3):e2023JC020338. https://doi.org/10.1029/2023JC020338

Smith KE, Burrows MT, Hobday AJ, et al (2021) Socioeconomic impacts of marine heatwaves: Global issues and opportunities. Science 374(6566):eabj3593. https://doi.org/10.1126/science.abj3593

Smith KE, Burrows MT, Hobday AJ, et al (2023) Biological impacts of marine heatwaves. Annual Review of Marine Science 15(1):119–145. https://doi.org/10.1146/annurev-marine-032122-121437

Tassone SJ, Besterman AF, Buelo CD, et al (2022) Co-occurrence of aquatic heatwaves with atmospheric heatwaves, low dissolved oxygen, and low pH events in estuarine ecosystems 45(3):707–720. https://doi.org/10.1007/s12237-021-01009-x

pandas development team T (2020) pandas-dev/pandas: Pandas. https://doi.org/10.5281/zenodo.3509134, URL https://doi.org/10.5281/zenodo.3509134

The Group for High Resolution Sea Surface Temperature Science Team, Piollé JF, Armstrong E, et al (2022) The recommended ghrsst data specification (gds) (gds 2.1 revision 0) https://doi.org/10.5281/zenodo.6984989

Tyrell T (2011) Anthropogenic modification of the oceans. Philosophical Transactions of the Royal Society A 369:887–908. https://doi.org/10.1098/rsta.2010.0334

Virtanen P, Gommers TERalf an Oliphant, Haberland M, et al (2020) SciPy 1.0: Fundamental Algorithms for Scientific Computing in Python. Nature Methods 17:261–272. https://doi.org/10.1038/s41592-019-0686-2

Wilks DS (2016) "The Stippling Shows Statistically Significant Grid Points": How Research Results are Routinely Overstated and Overinterpreted, and What to Do about It. Bulletin of the American Meteorological Society 97(12):2263–2273. https://doi.org/10.1175/BAMS-D-15-00267.1

Supplemental Material

Hovmöller: MUR, Geo-Polar, and OSTIA SST

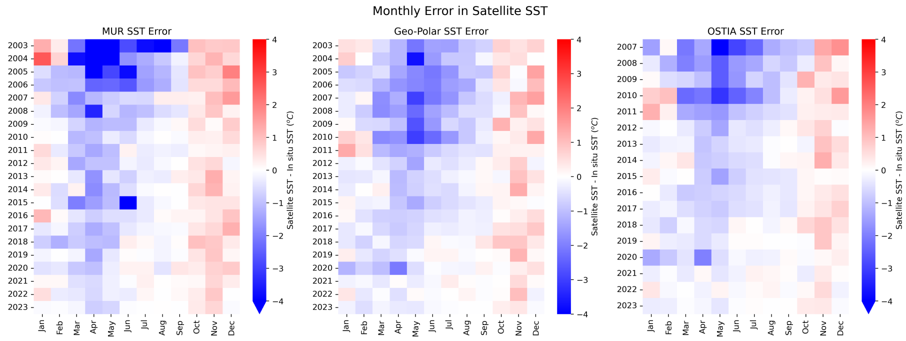

Fig. 17 The error in SST from climatology for NASA MUR, NOAA Geo-Polar, and Copernicus OSTIA by month and year. Each pixel corresponds to the average satellite error for all pixels in the Bay during that year (x axis) and month (y axis). The colorbar shows satellite SST minus in situ measurements, such that negative (blue) values represent satellite SST underestimates of in situ temperature. Geo-Polar SST has a long term trend in the error in SST anomaly from climatology over time in summer months, but no consistent seasonal error.

Hovmöller: MUR, Geo-Polar, and OSTIA SST Anomaly

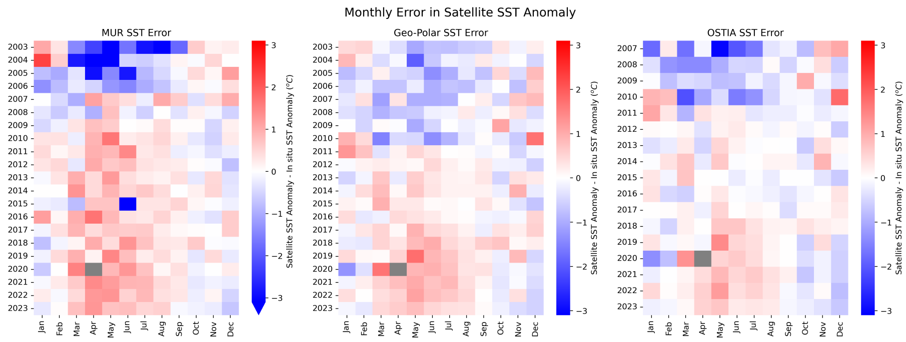

Fig. 18 The error in SST anomalies from climatology for NASA MUR, NOAA Geo-Polar, and Copernicus OSTIA by month and year. Each pixel corresponds to the average satellite error for all pixels in the Bay during that year (x axis) and month (y axis). The colorbar shows satellite SST anomaly minus in situ anomaly measurements, such that negative (blue) values represent satellite SST underestimates of in situ temperature anomaly.

Average Duration vs. Depth

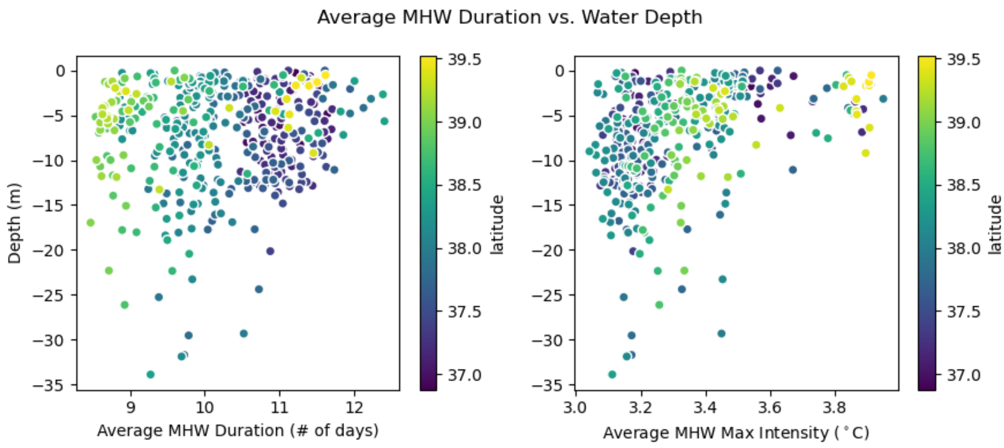

Fig. 19 Scatter plot showing the relationship between water depth and two marine heatwave characteristics: duration and maximum intensity. Both plots are colored by latitude, which serves as a visual approximation for which points are in the upper, middle, or lower Bay.